Decadal- to centennial-scale tropical Atlantic climate variability across a Dansgaard-Oeschger cycle

J. E. Hertzberg,[1,2] D. E. Black,[1] L. C. Peterson,[3] R. C. Thunell,[4] and G. H. Haug[5]

Received 25 October 2011; revised 5 July 2012; accepted 9 July 2012; published 24 August 2012.

[1] The patterns and forcing mechanisms of climate variability on decadal to centennial time scales represent a major void in our current understanding of Earth's climate system. Furthermore, the response of the low latitudes to abrupt climate change is also not well understood, as most high-resolution paleoclimate studies are from midlatitudes and high latitudes. This study explores the tropical Atlantic response to a Dansgaard-Oeschger cycle (Interstadial 12) using ultra-high resolution (~2–3 years) foraminiferal census data from Cariaco Basin sediments. The interpretation of the abundance records for the onset of Interstadial 12 is complicated by the competing effects of rising sea level on Ekman-induced upwelling within the Cariaco Basin and migrating Intertropical Convergence Zone–associated variations in trade wind location and fluvial nutrient delivery to the basin. The foraminiferal abundance records for the latter part of the interstadial suggest a southerly shift in the average annual position of the Intertropical Convergence Zone that acted to enhance upwelling and productivity within the Cariaco Basin. Sea level eventually reached a critical point in the transition back to stadial conditions that led to upwelling of nutrient-depleted waters and a decline in productivity within the basin. Spectral analyses of the *Globigerina bulloides* absolute abundance records reveal significant variability ranging from subdecadal- to centennial-scale. Atlantic multidecadal-scale climate variability is only evident in the warmest interval of Interstadial 12, suggesting that variability on this scale may only operate during warm climate periods, something that has significant implications for modern and near-future climate variability.

Citation: Hertzberg, J. E., D. E. Black, L. C. Peterson, R. C. Thunell, and G. H. Haug (2012), Decadal- to centennial-scale tropical Atlantic climate variability across a Dansgaard-Oeschger cycle, *Paleoceanography*, *27*, PA3218, doi:10.1029/2011PA002251.

1. Introduction

[2] Climate variability occurs on a number of different time scales, ranging from glacial-interglacial cycles to much shorter interannual fluctuations such as the El Niño–Southern Oscillation (ENSO). Early ice core records revolutionized our view of climate change with the discovery of Dansgaard-Oeschger (D-O) cycles in Greenland ice core data [*Dansgaard et al.*, 1982, 1993]. Originally thought to be restricted to the high-latitude North Atlantic, expressions of D-O cycles are found globally [*Voelker*, 2002; *Clement and Peterson*, 2008], including the subtropical Pacific [*Behl and Kennett*, 1996], the Gulf of California [*Schrader et al.*, 1980], the tropical Atlantic [*Peterson et al.*, 2000], and Antarctica [*Steig et al.*, 1998]. The high-latitude response to D-O cycles appears to be largely temperature-related [*Dansgaard et al.*, 1993; *Steig et al.*, 1998], but this is not the case at lower latitudes. For example, sediment records from the Santa Barbara and Guaymas Basins indicate variations in North Pacific Intermediate Water intensity and subsequent ventilation of eastern Pacific middepth waters across D-O cycles [*Schrader et al.*, 1980; *Behl and Kennett*, 1996].

[3] Studies from the Cariaco Basin using sediment reflectivity and trace element composition show variations in sediment organic carbon content and oxygenation of the basin's deep waters associated with D-O cycles [*Peterson et al.*, 2000]. Paired oxygen isotope and Mg/Ca paleothermometry records from the Cariaco Basin across Marine Isotope Stage (MIS) 3 indicate warmer and fresher conditions during interstadials, with an increase of ~3–4°C at stadial-interstadial transitions [*McConnell et al.*, 2007]. This study explores the tropical Atlantic response to a single D-O event (Interstadial 12 (IS12)) using ultrahigh resolution foraminiferal

[1]School of Marine and Atmospheric Sciences, Stony Brook University, Stony Brook, New York, USA.
[2]Now at Department of Oceanography, Texas A&M University, College Station, Texas, USA.
[3]Rosenstiel School of Marine and Atmospheric Science, University of Miami, Miami, Florida, USA.
[4]Department of Earth and Ocean Science, University of South Carolina, Columbia, South Carolina, USA.
[5]Geologisches Institut, ETH Zurich, Zurich, Switzerland.

Corresponding author: J. E. Hertzberg, Department of Oceanography, Texas A&M University, College Station, TX 77843, USA. (jhertzberg@ocean.tamu.edu)

0883-8305/12/2011PA002251

census data from Cariaco Basin sediments. The micropaleontological approach provides a different perspective on abrupt climate change in the tropics than previous geochemical-based reconstructions. Furthermore, and to the best of our knowledge, the high-resolution sampling performed as part of this study allows us to characterize subdecadal- to centennial-scale climate faunal variations at a higher resolution than any previous investigation of D-O cycles from the global marine archive.

2. Study Area

[4] The Cariaco Basin, situated on the northern continental shelf of Venezuela, is an ideal location to study past climate change on multiple time scales. It has served as the setting for numerous paleoclimate studies of the tropical Atlantic [e.g., *Peterson et al.*, 1991, 2000; *Hughen et al.*, 1996a; *Black et al.*, 1999, 2007; *Tedesco and Thunell*, 2003a; *Peterson and Haug*, 2006]. High-resolution climate reconstructions from the Cariaco Basin are possible because of the basin's high sediment accumulation rates and predominantly anoxic conditions, which result in the preservation of varves [*Hughen et al.*, 1996b].

[5] The basin is divided into two major subbasins, each reaching a maximum depth of ~1400 m, separated by a central saddle at ~900 m water depth [*Richards*, 1975; *Schubert*, 1982]. Modern connections to the Caribbean Sea occur via two shallow passages—the Centinela Channel in the northwest and the Tortuga Channel in the northeast, with water depths of 146 m and 135 m, respectively [*Alvera-Azcárate et al.*, 2009]. However, sea level was significantly lower during the focus of our study, with the sill depth likely fluctuating between 60 and 80 m. Today, surface waters within the basin can exchange freely with Caribbean surface waters, but waters below the sill depth are poorly ventilated.

[6] The Cariaco Basin sits near the northern limit of the annual latitudinal range of the Intertropical Convergence Zone (ITCZ) [*Haug et al.*, 2001]. Between January and March, the ITCZ is located in a position just south of the equator, and strong easterly trade winds blow along the northern coast of Venezuela leading to Ekman-induced upwelling of cool, nutrient-rich waters and high primary productivity [*Scranton et al.*, 2006]. This time of year is also the local dry season as the ITCZ and its associated precipitation lie far to the south. The intense upwelling during this period contrasts sharply with the diminished trade winds and weakened upwelling over the basin that accompanies the northward shift of the ITCZ during the Venezuelan rainy season, which begins in June or July. The regional rainy season also results in the enhanced delivery of terrigenous material to the basin from local rivers [*Peterson et al.*, 2000; *Martinez et al.*, 2010].

[7] The strong seasonal climatology is reflected in the biological variations within the surface waters of the Cariaco Basin, including that of the planktonic foraminifera. The spatial and temporal distributions of the planktonic foraminifera species are related to environmental parameters such as temperature, salinity, nutrients, and food supply [*Tedesco and Thunell*, 2003b]. Cariaco Basin sediment trap data collected between January 1997 and December 1999 quantified seasonal variations in planktonic foraminiferal flux and assemblage composition [*Tedesco and Thunell*, 2003b]. Nine species/varieties of planktonic foraminifera constitute >85% of the assemblage: *Orbulina universa*, *Globigerinoides ruber* (pink and white varieties), *Globigerina bulloides*, *Globigerina quinqueloba*, *Neogloboquadrina dutertrei*, *Globorotalia crassaformis*, *Globorotalia menardii*, and *Globigerinita glutinata* [*Tedesco and Thunell*, 2003b]. While these species are present throughout the year, their flux and relative contribution to the population vary both seasonally and interannually. This study will focus on three of these species: *G. bulloides*, *N. dutertrei*, and *G. ruber* (white).

3. Materials and Methods

[8] In May 2003, five Calypso piston cores were collected from the Cariaco Basin aboard the R/V *Marion Dufresne* as part of the Paléoclimatologie Isotopes CAlypso pour les Séries Sédimentaires Océaniques (PICASSO) campaign of the International Marine Past Global Change Study (IMAGES) XI program. MD03-2622 (10°42.69′ N 65°10.15′ W, 877 m water depth), the core used in this study, was recovered from the western side of the central saddle and has a length of 48.3 m. The core recovered a complete and continuous sequence spanning back through Termination II and into MIS 6. The average sedimentation rate for the entire core is 35 cm per thousand years. The core shows virtually no evidence of disturbance from the coring procedure, and an abundance of aragonitic pteropods in the recovered sediments indicates excellent carbonate preservation. This study explores the transitions into and out of IS12 (47,800 –~44,800 years BP), which was selected for its distinct "sawtooth" appearance in both the North Greenland Ice Core Project (NGRIP) $\delta^{18}O$ record [*Rasmussen et al.*, 2006] and sediment reflectivity data (Figures 1a and 1b). Sediment deposited during the stadial preceding IS12 is bioturbated, while sediment deposited during IS12 is visibly laminated throughout almost the entire interstadial (Figure 2) and largely devoid of benthic microfauna, indicating deposition under anoxic conditions. Focusing on the transitions into and out of IS12 allows us to compare conditions in the tropical North Atlantic across a period of abrupt warming and gradual cooling in the high-latitude North Atlantic.

[9] Sediment from IS12 was sampled at consecutive one mm intervals over the interval of 19.0 to 20.5 m in the core and freeze-dried. Approximately two thirds of each sample was rehydrated and disaggregated with deionized water, and then wet-sieved through a 63 μm mesh. The coarse fraction (>63 μm) was dried and sieved again through a 150 μm mesh. While all of the IS12 samples went through initial processing, foraminiferal census counts were performed on a subset of the samples (1 mm intervals from 19.96–20.50 m and 19.00–19.54 m), which cover the critical intervals spanning the onset and termination of IS12, respectively. For each sample in these intervals, the >150 μm fraction was split using a Sepor microsplitter until a suitable aliquot of at least 300 foraminifera was reached to minimize counting errors [*Imbrie and Kipp*, 1971]. The abundances of *Globigerina bulloides*, *Neogloboquadrina dutertrei*, *Orbulina universa*, *Globigerinella aequilateralis*, *Globorotalia crassaformis*, *Globorotalia menardii*, *Globigerinoides ruber* (pink and white varieties), *Globigerinoides sacculifer*,

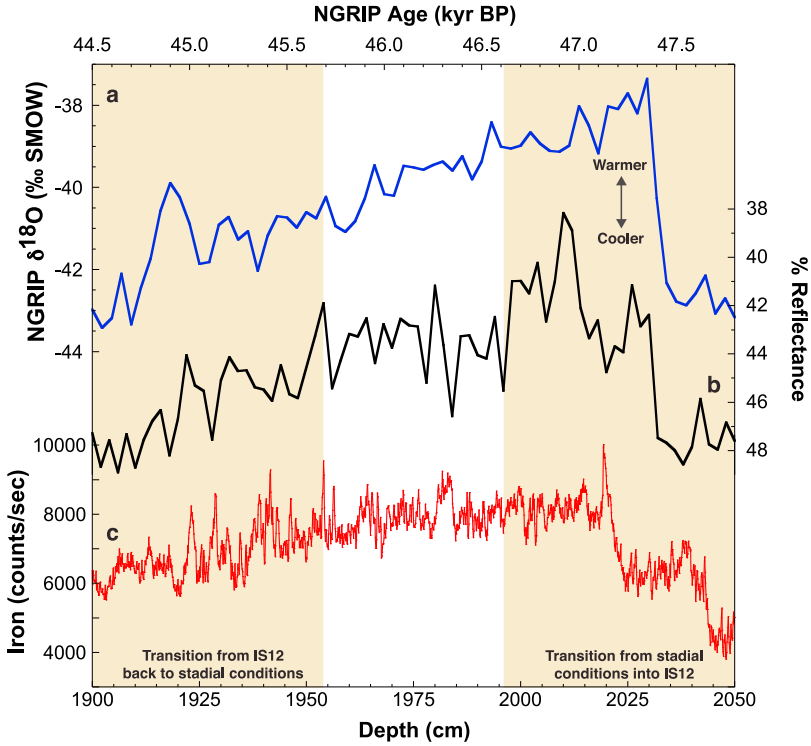

Figure 1. (a) NGRIP δ^{18}O record (blue line) used as a proxy for air temperature over Greenland [*Rasmussen et al.*, 2006]. More depleted δ^{18}O values indicate cooler temperatures, while enriched δ^{18}O values indicate warmer temperatures. (b) MD03-2622 sediment reflectivity (black line) across IS12, where darker, less reflective sediments are indicative of a higher content of organic matter. (c) MD03-2622 iron spectra (red line) across IS12 collected via XRF scanning. Beige shaded regions indicate the two sections of MD03-2622 where foraminiferal census data were collected. NGRIP δ^{18}O record is plotted against the NGRIP age model, while sediment reflectivity and iron spectra are plotted against depth in MD03-2622.

Globigerina rubescens, *Globorotalia truncatulinoides*, *Pulleniatina obliquiloculata*, *Globigerina quinqueloba*, and *Neogloboquadrina pachyderma* were determined using a standard binocular microscope. These are the most abundant foraminifera species in the Cariaco Basin sediment record, and the abundances of several of these species have been used in prior studies from the basin as significant indicators of past climate variability [*Overpeck et al.*, 1989; *Peterson et al.*, 1991; *Black et al.*, 1999]. Any other species present were grouped into an "other" category. Replicate counts were performed approximately every ten samples, and counting errors only involved misidentification of a single *G. bulloides* specimen in ten replicate samples. The minimum number of *G. bulloides* counted for any interval was 97 individuals, thus any potential counting error of this species would have a minimal overall impact on the total foraminiferal population of the sample. Relative and absolute abundances were then calculated from the foraminiferal census data to examine changes in the contribution of each species to the total assemblage, and the controls on the abundances of each individual species. The relative abundance is calculated as a percentage value of the total counted foraminiferal population,

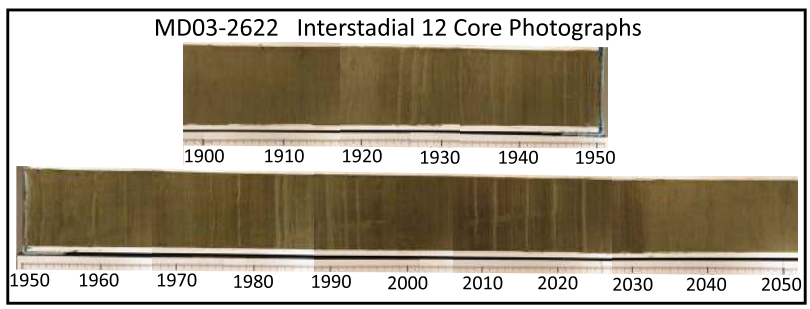

Figure 2. Composite photograph of sediment core MD03-2622 representing the interval that contains IS12 from 2050–1900 cm depth. Note the visible laminations in the core interval during IS12, suggesting that these sediments were deposited under anoxic conditions.

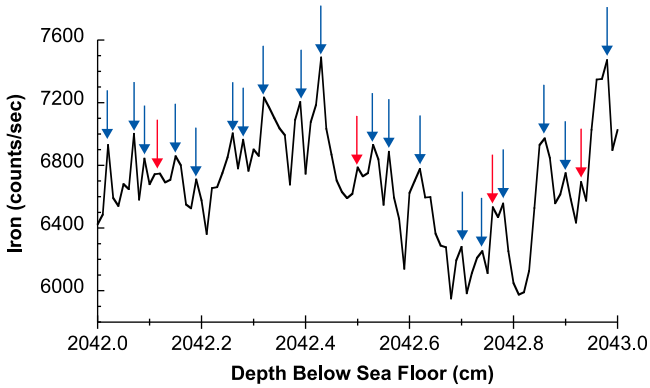

Figure 3. Example 10 mm section of sediment XRF iron counts used to establish a chronology for the IS12 section of MD03-2622. Blue arrows represent the minimum number of iron peaks counted in this section, and red arrows represent the additional peaks counted toward the maximum number of peaks in the section.

while the absolute abundance is calculated as the number of foraminifera normalized to per gram of dry sediment.

3.1. Age Model Development

[10] Prior studies have demonstrated that variations in Cariaco Basin sediment color are in phase and synchronous with Greenland climate change within the limits of dating error [*Hughen et al.*, 1996a; *Peterson et al.*, 2000]. On this basis, an initial age model for the IS12 section of the sediment core was created by visually matching tie points between the MD03-2622 sediment reflectance data and the well-dated North Greenland Ice Core Project (NGRIP) δ^{18}O chronology [*Rasmussen et al.*, 2006], and linearly interpolating between these points (Figures 1a and 1b). However, given the inherent error in visually matching tie points and the low resolution in which the sediment reflectivity data was collected, it was important to develop a more accurate, higher-resolution age model comparable to the resolution of the census data.

[11] To accomplish this, an "independent" age model for the IS12 section of MD03-2622 was created by examining downcore variations in elemental iron abundance throughout the section. Cariaco Basin sediments exhibit a distinct annual peak in iron abundance associated with increased delivery of terrigenous sediment during the regional rainy season [*Peterson et al.*, 2000; *Peterson and Haug*, 2006]. In principal, using sediment iron abundance in the core is analogous to counting tree rings—one should be able to determine the age of the sediments by counting yearly peaks in iron abundance. Elemental abundances of iron were measured for the IS12 core section using scanning X-ray fluorescence (XRF) at 100 μm intervals (Figure 1c). We divided the XRF data into 10 mm sections and counted what we considered the minimum and maximum number of iron peaks for each section (Figure 3). The minimum and maximum values for the 10 mm interval were then averaged to take into account that there may be more distinct peaks or even double peaks during some years, or weak and even no peaks during other years. Error for each section was calculated as the difference between the minimum and maximum year values for each 10 mm interval, and cumulative error upcore was calculated as the sum of the errors over preceding intervals. We excluded sections of core that contained visible microturbidites from our peak counts, which accounted for 65mm of the core section, or ~4% of the entire IS12 interval of MD03-2622. Finally, we pinned the base of our iron peak age model to a starting point in the NGRIP δ^{18}O chronology [*Rasmussen et al.*, 2006] using the sediment reflectivity correlation. At the top of our section of core, the difference between the iron-based age model and one based entirely on sediment reflectivity–NGRIP δ^{18}O correlations is 331 years (Figure 4). The cumulative error in the iron-based age model at the end of the section is +/−233 years, thus a minimum difference between the age models could be ~100 years. This is likely due to the inherent error in visually matching tie points between records, and the resolution differences in which the sediment reflectivity and ice core δ^{18}O data were collected. The iron-based chronology indicates that our 1 mm sampling results in a temporal resolution of approximately 2–3 years per sample, allowing for an unprecedented level of detail for a D-O cycle reconstruction.

4. Results

[12] Population data were collected for thirteen species of planktonic foraminifera. While we focus primarily on variations in *G. bulloides*, data from two other species, *N. dutertrei* and *G. ruber* (white), provide supporting information for the interpretation of the *G. bulloides* record. The remaining ten species either make up only a small portion of the total assemblage, or their population response to modern climate variability and hydrographic conditions is not sufficiently well understood to extrapolate into the past.

4.1. The Onset of Interstadial 12

[13] Foraminiferal census data were collected on 540 samples representing the preceding late stadial conditions (~47,800–47,400 years BP), the abrupt onset of IS12 (~47,400–47,250 years BP), and early IS12 (~47,250–46,660 years BP). In the late stadial preceding IS12, *G. bulloides* abundances (Figure 5e) fluctuate on centennial scales between ~500 *G. bulloides*/g and ~1,200 *G. bulloides*/g. From a relative percent perspective (Figure 6b), *G. bulloides* is the dominant species during stadial conditions, comprising between ~70–85% of the foraminiferal assemblage until the abrupt onset into IS12. During the transition into IS12, noted by the abrupt decline in sediment reflectance, *G. bulloides* abundances remain relatively constant at ~300 *G. bulloides*/g, while the species contribution to the total foraminiferal population declines abruptly from ~60 to 30%. During the early part of IS12, *G. bulloides* abundances gradually increase from ~200 *G. bulloides*/g to maximum values of ~1800 *G. bulloides*/g between 47,100–46,845 years BP before declining again. This peak in *G. bulloides* abundance at 46,845 years BP also corresponds to the peak in total foraminiferal abundance for the onset of IS12, with values reaching nearly 3,000 foraminifera/g (Figure 5b). *Globigerina bulloides* comprises ~40–60% of the foraminiferal assemblage during early IS12.

[14] Throughout the preceding late stadial the abundances of *N. dutertrei* (Figure 5f) do not vary significantly, averaging ~20 *N. dutertrei*/g, and the species does not contribute significantly to the total foraminiferal assemblage (Figure 6c). During the transition into IS12, abundances of

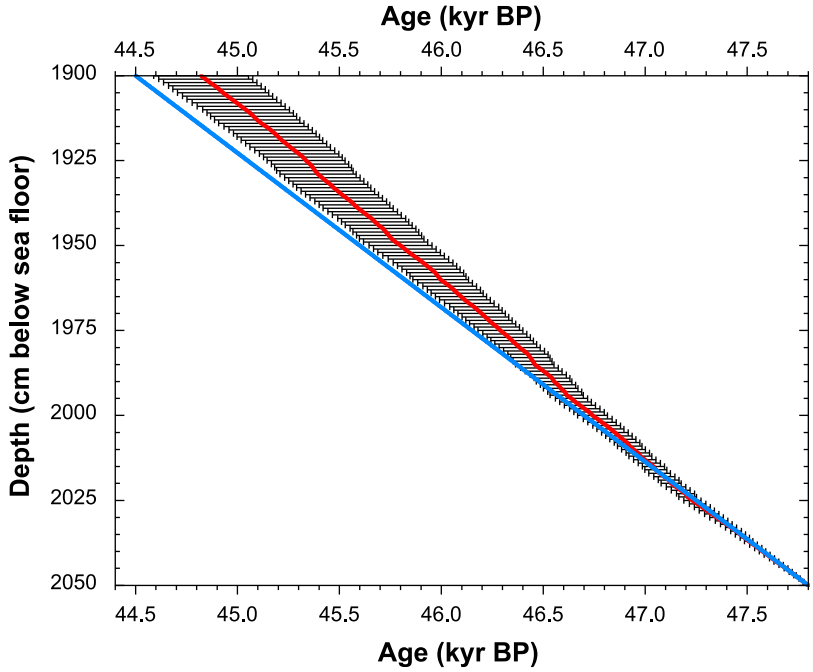

Figure 4. Age-depth comparisons of iron peak (red line with error bars) and reflectivity (blue line) based age models. Error bars were calculated as the difference between the minimum and maximum number of iron peaks for each 10 mm section. Cumulative error upcore was calculated as the sum of the current 10 mm section and the error of all of the preceding sections.

N. dutertrei rise abruptly, increasing by nearly an order of magnitude in less than 50 years and comprising ~50% of the foraminiferal population. After the species' abrupt increase during the transition into IS12, abundances and relative percent decline and remain low during early IS12, contributing ~10% to the foraminiferal assemblage.

[15] The abundances of *G. ruber* decline steadily over the preceding stadial and the transition into IS12 (Figure 5g), with relative percentages declining from ~7 to 2% (Figure 6d). Throughout early IS12, abundances of *G. ruber* are very low and *G. ruber* contributes ~1% to the foraminiferal assemblage.

4.2. The Transition out of Interstadial 12

[16] Foraminiferal census data were also collected on 540 samples representing the latter portion of IS12 and the transition into the following stadial (~45,885–44,820 years BP). The abundance record of *G. bulloides* for the latter part of IS12 (Figure 5e) begins relatively high although highly variable, and then values decrease between ~45,700 and 45,550 years BP. Abundances increase again at 45,450 years BP, peaking around 45,350 years BP, after which *G. bulloides* abundance values steadily decrease through the end of the interstadial and the transition back to stadial conditions. The relative percent of *G. bulloides* (Figure 6b) does not show any distinct long-term trends, but instead oscillates around a mean of 55%, with fluctuations never exceeding ~70% or dropping below ~35%.

[17] The *N. dutertrei* abundance record (Figure 5f) is very similar to that of *G. bulloides*. Abundance values start relatively high but variable before values decrease between ~45,700 to 45,500 years BP. Abundances increase again at ~45,450 years BP, peaking at ~45,350 years BP, after which *N. dutertrei* abundance values steadily decrease through the end of the interstadial. The contribution of *N. dutertrei* to the total foraminiferal population (Figure 6c) for late IS12 is ~20% and declines to ~10% on the transition back to stadial conditions. The major patterns of variability in the *G. bulloides* and *N. dutertrei* absolute abundance records (Figures 5e and 5f) closely match the overall total foraminiferal abundance (Figure 5b) for the transition out of IS12.

[18] The abundance record of white *G. ruber* during the IS12 termination (Figure 5g) contains two very abrupt peaks at ~45,340 years BP and ~45,400 years BP, and a smaller peak around ~45,525 years BP. Aside from these abundance maxima, abundance levels remain <~50 individuals/g for the remainder of the record. White *G. ruber* generally contributes <5% to the total foraminiferal population (Figure 6d), except for periods associated with the abundance peaks, at which time white *G. ruber* makes up ~20% of the total population. Relative percent values increase from <1% to ~10% during the early stadial conditions following IS12.

5. Discussion

[19] Several prior studies of Cariaco Basin sediments have used the abundances of planktonic foraminifera to reconstruct past climate variability [*Overpeck et al.*, 1989; *Peterson et al.*, 1991; *Black et al.*, 1999]. These studies focused on the abundance of *G. bulloides* as a proxy for upwelling and hence indirectly as an index for trade wind intensity and ITCZ position, although more recent work suggests that the Cariaco *G. bulloides* population can respond to local nutrient input from fluvial sources as well [*Peterson et al.*, 2000;

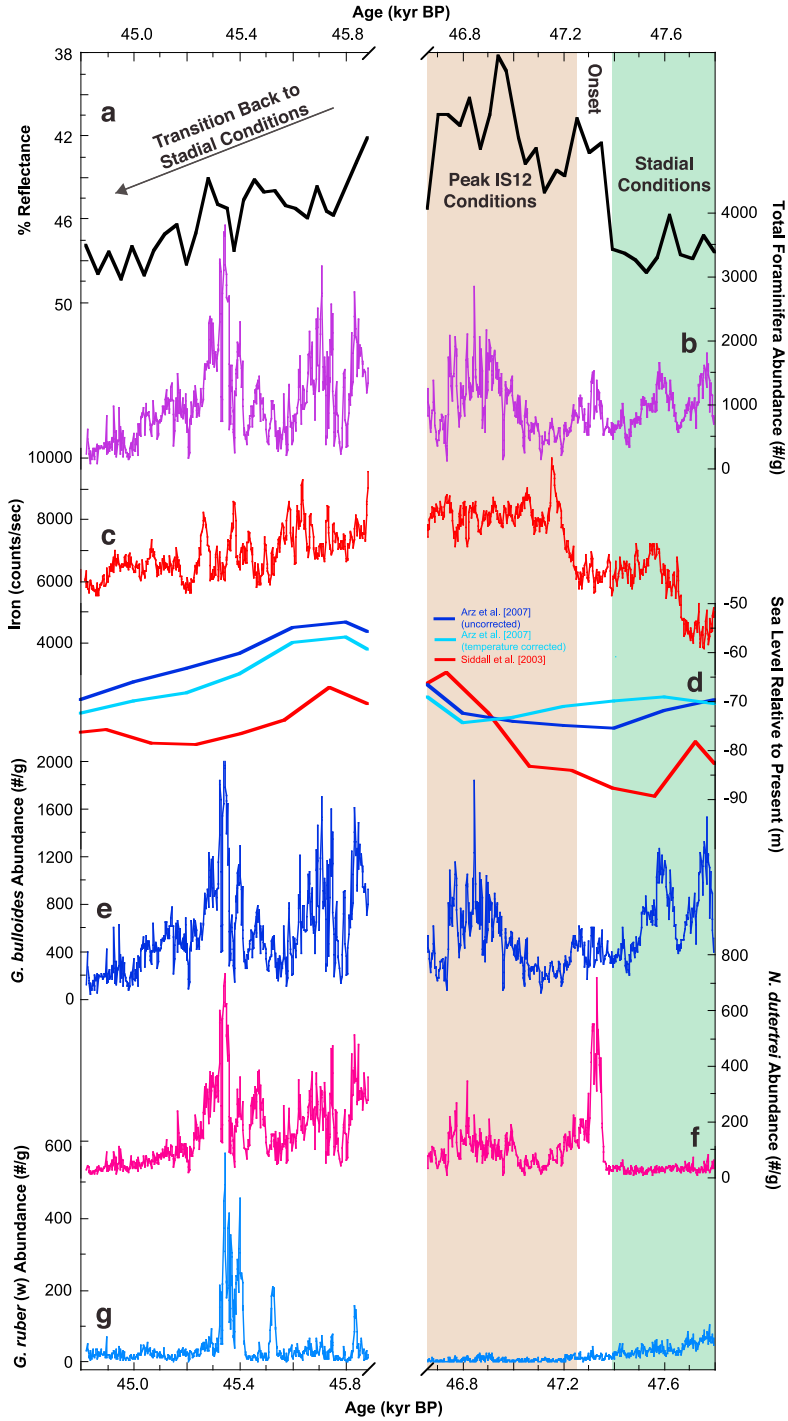

Figure 5. (a) MD03-2622 sediment reflectivity (black line) across IS12. (b) Absolute foraminiferal abundance (purple line) across IS12 expressed as the total number of foraminifera counted per sample per gram of sediment. (c) XRF iron spectra (red line) across IS12. (d) Records of global sea level change (expressed relative to present-day sea level) reconstructed from sediment cores from the Red Sea. *Siddall et al.* [2003] data (red line) are based on central Red Sea planktic foraminiferal isotopes, while *Arz et al.* [2007] data (blue lines) are based on northern Red Sea benthic isotopes. Both versions of the *Arz et al.* [2007] sea level records are plotted with the temperature corrected (light blue line) and uncorrected (dark blue line) data. Differences in the timing of the sea level changes in both records are likely due to the different methods in which the respective age models were constructed. (e) *Globigerina bulloides* (dark blue line), (f) *Neogloboquadrina dutertrei* (pink line), and (g) *Globigerinoides ruber* (white) (light blue line) absolute abundances calculated as the number of individuals per gram of sediment. Green shaded region indicates stadial conditions and beige shaded region indicates peak IS12 conditions.

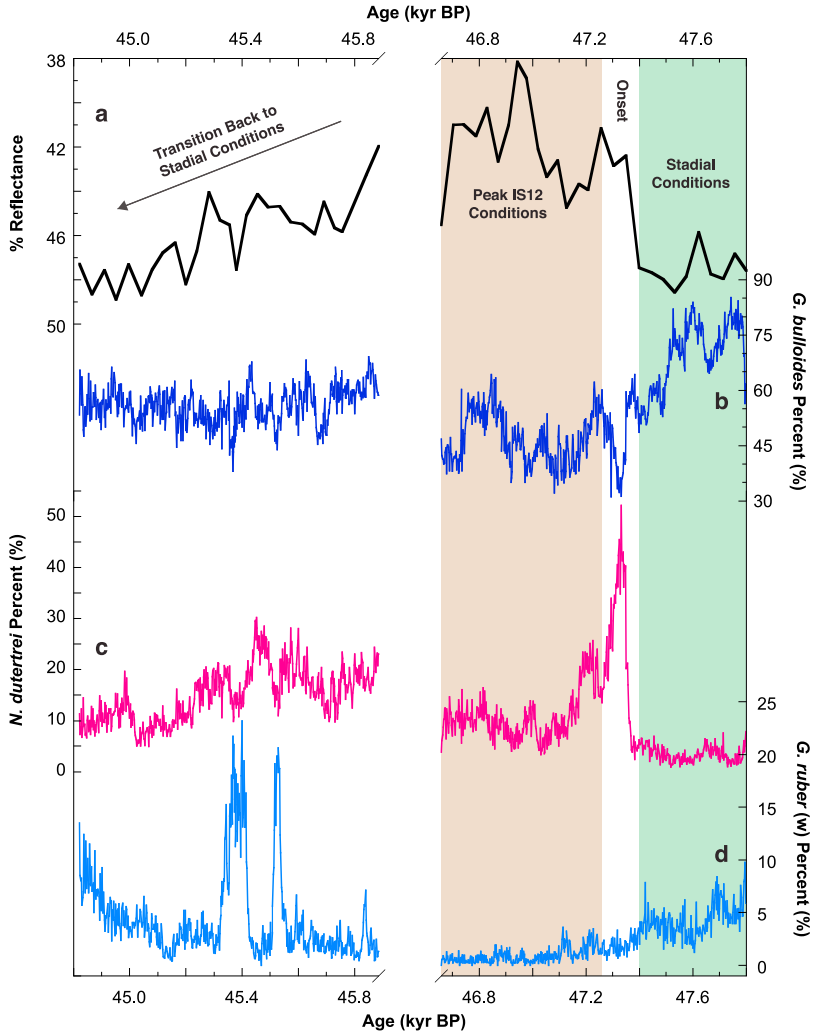

Figure 6. (a) MD03-2622 sediment reflectivity (black line) across IS12. (b) *Globigerina bulloides* (dark blue line), (c) *Neogloboquadrina dutertrei* (pink line), and (d) *Globigerinoides ruber* (white) (light blue line) relative abundances calculated as the percentage of each species to the total foraminifera population for each sample. Green shaded region indicates stadial conditions and beige shaded region indicates peak IS12 conditions.

Black et al., 2001]. We take a similar approach in interpreting the foraminiferal census records presented here, although we also bring two other species into the discussion: *N. dutertrei* and *G. ruber* (white). Within the Cariaco Basin, *G. bulloides* is the dominant planktonic foraminifera species during the modern upwelling season, with fluxes reaching ~4000 shells m^{-2} day^{-1} and comprising between 50% and 75% of the total flux during this period [*Tedesco and Thunell*, 2003b]. The abundance of *G. bulloides* is controlled primarily by variations in surface water productivity [*Thunell and Reynolds*, 1984; *Reynolds and Thunell*, 1985], thus its maximum flux and population contribution occur during the upwelling season. *Neogloboquadrina dutertrei* thrives in a well-stratified photic zone, and lives within the thermocline close to the chlorophyll maximum, a zone of high productivity and maximum food supply [*Fairbanks et al.*, 1982]. Chlorophyll values are highest in the basin during spring upwelling when the chlorophyll maximum shoals to 0–25 m [*Muller-Karger et al.*, 2001]; this period coincides with the peak flux of *N. dutertrei* [*Tedesco and Thunell*, 2003b]. *Globigerinoides ruber* inhabits the surface mixed layer [*Deuser*, 1987] and is most abundant in subtropical to tropical oligotrophic waters [*Miró*, 1971]. Like most taxa in the Cariaco Basin, *G. ruber* (white) experiences maximum flux during upwelling. However, this species accounts for less than 10% of the total annual flux, but constitutes 20–30% of the total assemblage when the percentage of *G. bulloides* is at a minimum and SSTs are beginning to decrease just prior to upwelling [*Tedesco and Thunell*, 2003b]. Using these species' ecological preferences we attempt to elucidate aspects of tropical Atlantic climate variability during IS12.

5.1. The Onset of Interstadial 12

[20] While previous studies have used *G. bulloides* abundance as a proxy for trade wind strength and ITCZ position, interpreting the *G. bulloides* abundance record at the onset of IS12 is not straightforward due to the competing effects of

rising sea level on Ekman-induced upwelling within the Cariaco Basin and migrating ITCZ-associated variations in trade wind location and fluvial nutrient delivery to the basin. The relationship between *G. bulloides* abundance and sediment reflectivity does not behave as expected (i.e., strongly correlated, Figures 5a and 5e), thus interpreting this species' abundance fluctuations strictly as an upwelling indicator should be treated with caution. Indeed, a previous study of Cariaco Basin sediments noted that carbonate accumulation, largely driven by foraminiferal productivity in the basin, was inversely correlated with sediment reflectivity [*Peterson et al.*, 2000]. Therefore, the relation between *G. bulloides* abundance and productivity appears more complex than originally thought.

[21] Sea level is thought to have been 90–95 m below present just prior to IS12 (Figure 5d) [*Siddall et al.*, 2003, 2008; *Rohling et al.*, 2008], comparable to sea level at 12,600 years BP (radiocarbon age) [*Fairbanks*, 1989]. It is important to note that we base our discussion of the effects of sea level on our records on the Red Sea reconstruction of *Siddall et al.* [2003], as a later reconstruction from the Red Sea [*Arz et al.*, 2007] using a different method obtained slightly different magnitudes and overall sea level changes across IS12 (Figure 5d). *Peterson et al.* [1991] suggested that the Cariaco Basin upwelling zone was displaced to the north, outside of the Cariaco Basin prior to 12,600 years BP as a result of significantly lower sea level, exposure of the Unare Platform to the south, and resulting effects on Ekman dynamics within the basin under low-stand conditions. In addition, diminished productivity has been inferred for the stadial preceding IS12 based on low dinoflagellate cyst accumulation in Cariaco Basin sediments of that age [*González et al.*, 2008]. Under modern conditions in the Cariaco Basin, high-nitrate Subtropical Underwater (SUW) enters the basin and is brought to the surface during the spring upwelling season, elevating nutrient concentrations in the upper water column and stimulating phytoplankton growth [*Muller-Karger et al.*, 2001]. It has been suggested that periods of reduced productivity in the Cariaco Basin during MIS 3 are likely due to shallow sill depths, inhibiting the inflow of Subtropical Underwater and restricting the availability of nutrients [*González et al.*, 2008]. In addition, studies from the Bahama Bank and central Caribbean suggest that SUW was depleted in nutrients during glacial intervals [*Slowey and Curry*, 1995; *Kameo et al.*, 2004], with even greater nutrient depletions during Heinrich Events [*Vink et al.*, 2001]. However, *G. bulloides* abundances during the late-stadial preceding IS12 are not distinctly lower than those observed during and after the interstadial onset (Figure 5e); in fact, they are greater. Furthermore, percentages of *G. bulloides* are higher during the late-stadial and decline as one moves into the interstadial (Figure 6b), showing an inverse correlation with sediment reflectivity. While it is possible that *G. bulloides* was able to outcompete companion foraminifera species during reduced productivity conditions, this would be the opposite of what is observed in the basin today [*Tedesco and Thunell*, 2003b].

[22] Sea level increased 20–30 m across IS12 (Figure 5d) [*Siddall et al.*, 2003], raising sill depths equivalent to those experienced during the Younger Dryas, a time when upwelling did occur within the Cariaco Basin [*Hughen et al.*, 1996a]. If one looks at the onset of IS12 only after the rise in sediment reflectivity, *G. bulloides* abundance follows the same trend—as sediments get richer in organic carbon (i.e., darker and less reflective), *G. bulloides* abundance increases. This still leaves the relatively high *G. bulloides* abundances during the late-stadial without a clear explanation, at least from the perspective of upwelling variability.

[23] Another possible control on *G. bulloides* abundance, albeit an indirect one, is fluvial nutrient delivery through the onset of IS12. An argument for increased fluvial input to the basin at the IS12 onset is supported by census data from *N. dutertrei* and *G. ruber* (white). *Neogloboquadrina dutertrei* prefers a well-stratified photic zone, where it dwells in the thermocline, close to the chlorophyll maximum [*Fairbanks et al.*, 1982]. Abundances of *N. dutertrei* shift to very high values just after the abrupt transition into the interstadial (Figure 5f). It is clear that an ecological threshold was reached which contributed to *N. dutertrei* flourishing at this point. Given what we know about the preferred habitat of *N. dutertrei*, its abundance pattern suggests an increasingly stratified water column, most likely on a seasonal basis, resulting from a climatically sudden increase in boreal summer/fall precipitation as the ITCZ migrated north. Abundance and relative percent data for *N. dutertrei* display nearly identical patterns, suggesting that variations in this species' abundance play a role in driving the relative percent of other species in the assemblage. The abundance patterns of *G. ruber* (white) also support the notion of increased fluvial input to the basin at the interstadial onset. The white variety of *G. ruber* is a tropical to subtropical species that inhabits the surface mixed layer between 0 and 45 m water depth [*Deuser*, 1987; *Bé*, 1982], and is most abundant in oligotrophic waters [*Fairbanks et al.*, 1982]; it reaches maximum abundances in regions where salinity is relatively high [*Kemle-von Mücke and Oberhänsli*, 1999]. The gradual decline in *G. ruber* at the transition into IS12 (Figure 5g) is likely related to a combination of reduced salinity as regional precipitation and fluvial flow to the basin increased, and the resultant change from oligotrophic waters to more eutrophic conditions with increased productivity. *Neogloboquadrina dutertrei* shows an abrupt response to the IS12 onset as the species was able to take advantage of the increased productivity associated with enhanced fluvial input of nutrients at the onset of IS12. *Globigerinoides ruber* populations may have been weak during the preceding stadial as a result of shallower sill depths and decreased food supply associated with upwelling of nutrient-depleted water. An increase in fluvial input to the basin at the onset of IS12 would have led to a further decline in *G. ruber* populations due to decreased surface water salinity and more eutrophic conditions.

[24] One of the goals of this study was to explore the nature of decadal- to centennial-scale variability in the tropical Atlantic during a time when boundary conditions were very different from today. To that end we performed multitaper spectral analysis on the *G. bulloides* abundance data to identify significant modes of variability. We divided the onset of IS12 into two sections for spectral analysis to allow us to directly compare stadial versus interstadial conditions: the period from 47,800 to 47,398 years BP represents the late-stadial interval just prior to IS12, and the period from 47,398 to 46,658 years BP represents the abrupt transition into IS12. For the late stadial period prior to the beginning of IS12, spectral analysis reveals concentrations

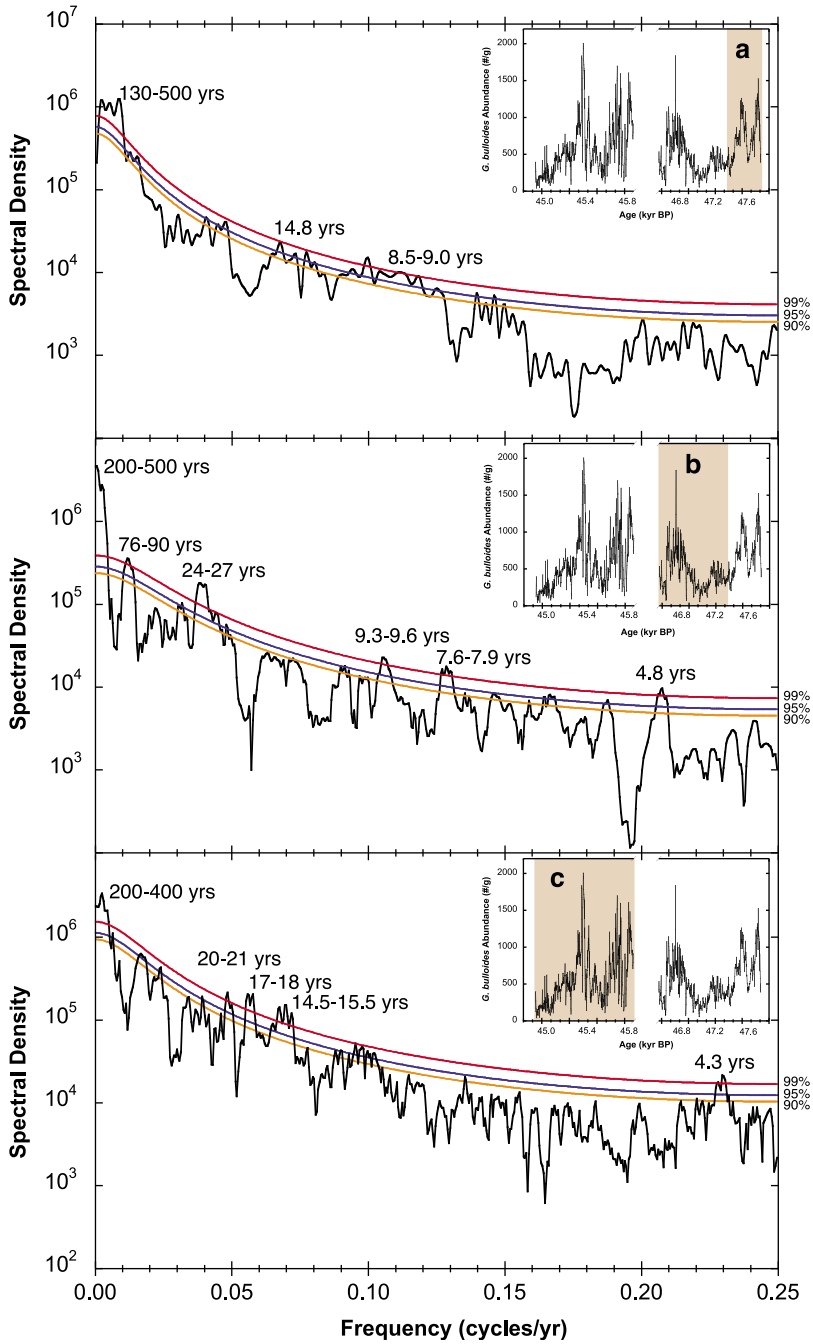

Figure 7. Spectral analyses for the (a) stadial period prior to IS12, (b) transition into IS12 and peak IS12 conditions, and (c) the transition out of IS12 back to stadial conditions. Inset in each panel shows the corresponding section of the *G. bulloides* abundance data used for the analysis (beige shading in inset). Red, blue, and orange lines indicate the 99, 95, and 90% confidence intervals, respectively. For spectral peaks at or above the 99% confidence interval (red line), frequencies are converted to period and labeled above the peak.

of variance above the 99% confidence level in subdecadal to decadal modes (8.5 to 9.0 years and 14.8 years) and a multicentennial mode (130 to 500 years) (Figure 7a) that is poorly defined due to the length of the late stadial portion of the record (402 years).

[25] The 8.5 to 9.0 year period is comparable to that associated with the North Atlantic Oscillation (NAO). In the modern climate system the NAO is strongly correlated with midlatitude variability but only weakly correlated with tropical Atlantic variability [*Marshall et al.*, 2001]. Given that the period prior to the abrupt onset into IS12 was a cold stadial interval, the NAO influence likely extended further south than its modern latitudinal extent. If the ITCZ had taken a more southerly average annual position during the stadial prior to IS12 [*Peterson et al.*, 2000; *Schmidt and Spero*, 2011], major atmospheric circulation cells and the

latitudinal influence of the NAO may have shifted south in response. Thus, while the influence of the NAO in the modern climate system is weakly correlated to the tropical Atlantic, it is possible its influence was stronger in the tropics during cold stadials of the last glacial period in response to a shift in large-scale atmospheric circulation.

[26] A distinctly different spectral pattern emerges from the early IS12 data. Here, concentrations of variance above the 99% confidence level occur in interannual (4.8 years and 7.6 to 7.9 years), decadal to interdecadal (9.3 to 9.6 years and 24 to 27 years), multidecadal (76 to 90 years), and multicentennial modes (200 to 500 years) (Figure 7b). Like the prior stadial interval, it is difficult to make any significant inferences about the multicentennial mode given the length of the available time series (740 years). Unlike the colder stadial interval, the warmer interstadial displays significant interannual, interdecadal, and multidecadal variability. When compared to a spectrum of modern *G. bulloides* abundance [*Black et al.*, 1999], the largest difference is a pronounced multidecadal mode in the IS12 record.

[27] The interannual variability observed during the IS12 onset could be related to either the El Niño–Southern Oscillation (ENSO) [e.g., *Hughen et al.*, 1999; *Tudhope et al.*, 2001], or a phenomenon that is similar to ENSO, but weaker, known as the Atlantic Niño [*Latif and Grotzner*, 2000]. Analyses of instrumental data suggest that ENSO exerts a prominent influence on the tropical North Atlantic, primarily through variations in latent heat flux during the spring following an El Niño [*Chang et al.*, 2006]. However, previous paleoclimate records from the Cariaco Basin spanning the last millennium have not been able to identify specific large-magnitude El Niño events [e.g., *Black et al.*, 1999, 2007]. Alternatively, warm events of the Atlantic Niño reach their maximum strength in the latter half of the year, with manifestations focused primarily near the equator [*Latif and Grotzner*, 2000; *Wang*, 2002]. During the warm phase, trade winds in the equatorial western Atlantic are weak and SST is high in the eastern equatorial Atlantic. Ascending motion associated with the Gulf of Mexico/Caribbean Sea–Amazon heat source extends eastward and weakens the Atlantic Walker circulation. This decreases surface equatorial easterly wind in the western Atlantic, which in turn further increases SST in the equatorial eastern Atlantic [*Wang*, 2005]. The reverse occurs during a cold phase. The Atlantic Niño is mostly independent of ENSO variability with a shorter characteristic time scale and is not related to the tropical Atlantic response to the Pacific ENSO. It has also been observed that the Atlantic Hadley circulation strengthens during the warm phase of the Atlantic Niño [*Wang*, 2005]. It is more likely that the interannual variability in the *G. bulloides* time series from IS12 is related to the Atlantic Niño as the impacts are more direct. However, the Atlantic Niño has an observed period range of 3–5 years [*Chang et al.*, 2006], which is at the Nyquist frequency of our record, thus it is not possible to make interpretations about Atlantic Niño variability based solely on the spectral analysis results alone.

[28] The multidecadal variability in the *G. bulloides* time series for the latter interval of the onset of IS12 may be related to something similar to the modern Atlantic Multidecadal Oscillation (AMO). The AMO, which has a period of ~60–80 years, is highly correlated with tropical Atlantic climate patterns such as rainfall in the Nordeste of Brazil and the African Sahel, as well as Atlantic hurricane variability [*Knight et al.*, 2006]. Some studies have suggested that multidecadal variability in the North Atlantic is related to fluctuations in Atlantic meridional overturning circulation (AMOC) [*Latif et al.*, 2004; *Knight et al.*, 2006]. Stadial conditions such as those experienced during the earliest portion of our record may represent a state where AMOC is in a stable "off" mode [*Broecker et al.*, 1985, 1990], and that instabilities in the coupled ocean-atmosphere system are introduced when AMOC intensifies. Given that multidecadal variability is not present during the earlier interval prior to the onset of IS12, it is possible that multidecadal climate fluctuations similar to the AMO operate primarily during warm climate intervals, something that has significant implications for modern and near-future climate variability. The observed decadal and interdecadal modes of variability during the onset of IS12 (for both the earlier and latter intervals) represent periodicities that have no modern analogs, thus it is difficult to infer what climate phenomena they may be related to. As IS12 occurred under boundary conditions that are different from today it is likely that there were modes of climate variability during IS12 that we do not see in the modern climate system.

[29] Cross-spectral analyses (not shown) were performed between the XRF iron spectra data and the absolute abundance records of all three species (*G. bulloides, N. dutertrei*, and *G. ruber* (white)) to determine whether the records contain statistically similar frequency components. For these analyses, the onset of IS12 was not split into two separate intervals. Both *G. bulloides* and *N. dutertrei* display spectral coherency with the iron data, with coherent peaks above the 80% confidence interval for several periods between 4 and 7 years. Spectral coherency between *N. dutertrei* and the iron data is also evident at longer periods (8, 10, and 14 years); however, these may be harmonics of shorter periods. Cross-spectral analysis between *G. ruber* abundance and the iron spectra did not yield any statistically significant spectral coherency. The coherent peaks between both the *G. bulloides* and *N. dutertrei* and the iron spectra data between 4 and 7 years suggests that the dominant driver of variability on these periods is either ENSO or the Atlantic Niño.

5.2. The Transition out of Interstadial 12

[30] The latter portion of the study interval in MD03-2622 represents the gradual transition out of IS12 and back to stadial conditions. As already discussed, the interpretation of the *G. bulloides* record for the onset of IS12 is not straightforward as the transition into the interstadial was marked by abruptly rising sea level and its influence on upwelling within the basin, and a rapid northerly shift in ITCZ position, also influencing upwelling in the Cariaco. Unlike the IS12 onset, *G. bulloides* absolute abundances for the transition out of IS12 and back to stadial conditions more closely follows changes in sediment reflectivity across the transition. The contrast in behavior is probably due to the upwelling zone remaining within the basin at the end of the interstadial. IS12 occurred after Heinrich event 5, amplifying the initial sea level rise. While sea level rose between 20 and 30 m during the transition into IS12 (a level equivalent to 60–70 m below present levels), sea level regressed only ~10 m (a level equivalent to 70–80 m below present levels) during the more

gradual transition out of the interstadial (Figure 5d) [*Siddall et al.*, 2003]. Thus, *G. bulloides* absolute abundance and sediment reflectivity indicate a gradual decline in upwelling intensity at the end of the interstadial (Figures 5a and 5e), eventually leading to the transition back to oxic conditions within the basin. One complicating factor in this interpretation is that while gradually declining sea level would have slowly cut off the external nutrient supply to the basin, the ITCZ was also shifting southward [*Peterson et al.*, 2000], something that should have enhanced upwelling within the Cariaco Basin. Declining values for both *G. bulloides* absolute abundance and sediment reflectivity after ~45,300 years BP may be due to sea level reaching a critical point for diminishing nutrient supply, with the century-long pulse in *G. bulloides* abundance just prior to this time representing a last surge of ITCZ migration-related upwelling before surface nutrient input from the Caribbean Sea to the basin was effectively removed. This is not to say upwelling was necessarily reduced, but rather the water being upwelled was nutrient-depleted. In addition, the southward shift of the ITCZ during stadials acted to decrease regional precipitation around the Cariaco Basin, resulting in a decrease in fluvially derived nutrients [*Peterson et al.*, 2000].

[31] The absolute abundance record of *N. dutertrei* for the latter part of IS12 is nearly identical to that of *G. bulloides*, suggesting that the same forcing mechanism is likely driving the patterns seen in both records. While *N. dutertrei* may prefer a highly stratified water column, it also inhabits a region close to the chlorophyll maximum, thus its response to upwelling during the latter part of IS12 may be due to increased phytoplankton driven by enhanced upwelling. Therefore, *G. bulloides* and *N. dutertrei* likely exhibit similar patterns during this interval as both are responding to enhanced upwelling. This is in contrast to the onset of IS12 when *N. dutertrei* abundances were likely driven by an abrupt onset of stratification within the basin as the ITCZ migrated northward. Indeed, the highest fluxes of *N. dutertrei* in the modern Cariaco Basin have been shown to occur during the upwelling season [*Tedesco and Thunell*, 2003b].

[32] As was done for the *G. bulloides* abundance record for the onset of IS12, multitaper spectral analysis was performed on the *G. bulloides* abundance record for the IS12 termination. The spectral analysis was performed on the full record of the transition out of IS12 (45,885 to 44,821 years BP). Concentrations of variance occur in interannual (4.3 years), decadal to interdecadal (14.5–15.5 years, 17–18 years, 20–21 years), and multicentennial (200–400 years) modes (Figure 7c). The interannual variance in the record is again possibly related to the Atlantic Niño and its associated influence on the trade wind system, although ENSO cannot be ruled out if it existed at the time. Similar to the IS12 onset, the decadal and interdecadal modes for the IS12 termination have no modern analogs, thus it is difficult to infer what climate phenomena they may be related to. The lack of pronounced multidecadal variability in both the preceding stadial (Figure 7a) and during the IS12 termination again strongly suggests that AMO-type variability may only operate during relatively warm climate periods.

6. Conclusions

[33] We present foraminiferal census data from the Cariaco Basin spanning the onset and termination of IS12 at a temporal resolution of 2–3 years, making this one of the most detailed records of climate variability across a D-O cycle to date. Our results support a northward shift of the ITCZ associated with the interstadial onset first noted in Cariaco sediment reflectance studies [*Peterson et al.*, 2000]. However, the productivity history within the Cariaco Basin is complicated due to the combined effects of ITCZ migration and rising sea level. The transition out of IS12 behaves as one might expect, with *G. bulloides* abundance generally tracking sediment reflectivity, and hence sediment organic carbon content. Multidecadal variability similar to the AMO in scale was only noted during the warmest part of the interstadial, and thus may be a function of relatively warm climate states, while being absent during colder, stadial and near-stadial conditions.

[34] **Acknowledgments.** We thank Jennifer Wurtzel for computational assistance and Matthew Schmidt for insightful discussions. We also thank two anonymous reviewers for their valuable comments. This work was supported by NSF grants OCE06-02376 to D. Black, OCE06-02392 to L. Peterson, and OCE06-02316 to R. Thunell.

References

Alvera-Azcárate, A., A. Barth, and R. H. Weisberg (2009), A nested model of the Cariaco Basin (Venezuela): Description of the basin's interior hydrography and interactions with the open ocean, *Ocean Dyn.*, *59*, 97–120, doi:10.1007/s10236-008-0169-y.

Arz, H. W., F. Lamy, A. Ganopolski, N. Nowaczyk, and J. Pätzold (2007), Dominant Northern Hemisphere climate control over millennial-scale glacial sea-level variability, *Quat. Sci. Rev.*, *26*(3–4), 312–321, doi:10.1016/j.quascirev.2006.07.016.

Bé, A. W. H. (1982), Biology of planktonic foraminifera, in *Foraminifera: Notes for a Short Course, Studies in Geology*, vol. 6, edited by T. Broadhead, pp. 51–92, Univ. of Tennessee, Knoxville.

Behl, R. J., and J. P. Kennett (1996), Brief interstadial events in the Santa Barbara Basin, NE Pacific, during the past 60 kyr, *Nature*, *379*, 243–246, doi:10.1038/379243a0.

Black, D. E., R. C. Thunell, A. Kaplan, L. C. Peterson, and E. J. Tappa (2001), High-resolution records of tropical Atlantic climate variability from the Cariaco Basin, paper presented at GSA Annual Meeting, Geol. Soc. of Am., Boston, Mass.

Black, D. E., L. C. Peterson, J. T. Overpeck, A. Kaplan, M. N. Evans, and M. Kashgarian (1999), Eight centuries of North Atlantic Ocean atmosphere variability, *Science*, *286*, 1709–1713, doi:10.1126/science.286.5445.1709.

Black, D. E., M. A. Abahazi, R. C. Thunell, A. Kaplan, E. J. Tappa, and L. C. Peterson (2007), An 8-century tropical Atlantic SST record from the Cariaco Basin: Baseline variability, twentieth-century warming, and Atlantic hurricane frequency, *Paleoceanography*, *22*, PA4204, doi:10.1029/2007PA001427.

Broecker, W. S., D. Peteet, and D. Rind (1985), Does the ocean-atmosphere system have more than one stable mode of operation?, *Nature*, *315*, 21–26, doi:10.1038/315021a0.

Broecker, W. S., G. Bond, M. Klas, G. Bonani, and W. Wolfli (1990), A salt oscillator in the glacial Atlantic? 1. The concept, *Paleoceanography*, *5*, 469–477, doi:10.1029/PA005i004p00469.

Chang, P., et al. (2006), Climate fluctuations of tropical coupled systems: The role of ocean dynamics, *J. Clim.*, *19*, 5122–5174, doi:10.1175/JCLI3903.1.

Clement, A. C., and L. C. Peterson (2008), Mechanisms of abrupt climate change of the last glacial period, *Rev. Geophys.*, *46*, RG4002, doi:10.1029/2006RG000204.

Dansgaard, W., H. B. Clausen, N. Gundestrup, C. U. Hammer, S. F. Johnsen, P. M. Kristinsdottir, and N. Reeh (1982), A new Greenland deep ice core, *Science*, *218*, 1273–1277, doi:10.1126/science.218.4579.1273.

Dansgaard, W., et al. (1993), Evidence for general instability of past climate from a 250-kyr ice-core record, *Nature*, *364*, 218–220, doi:10.1038/364218a0.

Deuser, W. G. (1987), Seasonal-variations in isotopic composition and deep-water fluxes of the tests of perennially abundant planktonic-foraminifera of the Sargasso Sea - Results from sediment-trap collections and their paleoceanographic significance, *J. Foraminiferal Res.*, *17*, 14–27, doi:10.2113/gsjfr.17.1.14.

Fairbanks, R. G. (1989), A 17,000-year glacio-eustatic sea level record: Influence of glacial melting rates on the Younger Dryas event and deep-ocean circulation, *Nature*, *342*, 637–642, doi:10.1038/342637a0.

Fairbanks, R. G., M. Sverdlove, R. Free, P. H. Wiebe, and A. W. H. Bé (1982), Vertical-distribution and isotopic fractionation of living planktonic-foraminifera from the Panama Basin, *Nature*, *298*, 841–844, doi:10.1038/298841a0.

González, C., L. M. Dupont, K. Mertens, and G. Wefer (2008), Reconstructing marine productivity of the Cariaco Basin during marine isotope stages 3 and 4 using organic-walled dinoflagellate cysts, *Paleoceanography*, *23*, PA3215, doi:10.1029/2008PA001602.

Haug, G. H., K. A. Hughen, D. M. Sigman, L. C. Peterson, and U. Röhl (2001), Southward migration of the intertropical convergence zone through the Holocene, *Science*, *293*, 1304–1308, doi:10.1126/science.1059725.

Hughen, K. A., J. T. Overpeck, L. C. Peterson, and S. Trumbore (1996a), Rapid climate changes in the tropical Atlantic region during the last deglaciation, *Nature*, *380*, 51–54, doi:10.1038/380051a0.

Hughen, K. A., J. T. Overpeck, L. C. Peterson, and R. F. Anderson (1996b), The nature of varved sedimentation in the Cariaco Basin, Venezuela, and its palaeoclimatic significance, in *Palaeoclimatology and Palaeoceanography From Laminated Sediments*, edited by A. E. S. Kemp, *Geol. Soc. Spec. Publ.*, *116*, 171–183, doi:10.1144/GSL.SP.1996.116.01.15.

Hughen, K. A., D. P. Schrag, S. B. Jacobsen, and W. Hantoro (1999), El Niño during the last interglacial period recorded by a fossil coral from Indonesia, *Geophys. Res. Lett.*, *26*, 3129–3132, doi:10.1029/1999GL006062.

Imbrie, J., and N. G. Kipp (1971), A new micropaleontological method for quantitative paleoclimatology: Application to a late Pleistocene Caribbean core, in *The Late Cenozoic Glacial Ages*, edited by K. Turekian, pp. 71–181, Yale Univ. Press, New Haven, Conn.

Kameo, K., M. Shearer, A. W. Drozler, I. Mita, R. Watanabe, and T. Sato (2004), Glacial-interglacial surface water variations in the Caribbean Sea during the last 300 ky based on calcareous nannofossil analysis, *Palaeogeogr. Palaeoclimatol. Palaeoecol.*, *212*, 65–76.

Kemle-von Mücke, S., and H. Oberhänsli (1999), The distribution of living planktonic foraminifera in relation to Southeast Atlantic oceanography, in *Use of Proxies in Paleoceanography: Examples from the South Atlantic*, edited by G. Fischer and G. Wefer, pp. 91–115, Springer, Berlin, doi:10.1007/978-3-642-58646-0_3.

Knight, J. R., C. K. Folland, and A. A. Scaife (2006), Climate impacts of the Atlantic Multidecadal Oscillation, *Geophys. Res. Lett.*, *33*, L17706, doi:10.1029/2006GL026242.

Latif, M., and A. Grotzner (2000), The equatorial Atlantic oscillation and its response to ENSO, *Clim. Dyn.*, *16*, 213–218, doi:10.1007/s003820050014.

Latif, M., E. Roechner, M. Botzet, M. Esch, H. Haak, S. Hagemann, J. Jungclaus, S. Leguthke, S. Marsland, and U. Mikolajewicz (2004), Reconstructing, monitoring, and predicting multidecadal-scale changes in the North Atlantic thermohaline circulation with sea surface temperature, *J. Clim.*, *17*, 1605–1614, doi:10.1175/1520-0442(2004)017<1605:RMAPMC>2.0.CO;2.

Marshall, J., Y. Kushnir, D. Battisti, P. Chang, A. Czaja, R. Dickinson, J. Hurrell, M. McCartney, R. Saravanan, and M. Visbeck (2001), North Atlantic climate variability: Phenomena, impacts and mechanisms, *Int. J. Climatol.*, *21*, 1863–1898, doi:10.1002/joc.693.

Martinez, N. C., R. W. Murray, R. C. Thunel, L. C. Peterson, F. Muller-Karger, L. Lorenzoni, Y. Astor, and R. Varela (2010), Local and regional geochemical signatures of surface sediments from the Cariaco Basin and Orinoco Delta, Venezuela, *Geology*, *38*, 159–162, doi:10.1130/G30487.1.

McConnell, M., R. Thunell, L. Peterson, D. Black, and D. Lea (2007), Tropical climate variability during Marine Isotope Stage 3: Results from the Cariaco Basin, *Eos Trans. AGU*, *88*(52), Fall Meet. Suppl., Abstract OS43C-05.

Miró, M. (1971), Los foraminiferos planctonicos vivos y sedimentados del margen continental de Venezuela, *Acta Geol. Hisp.*, *VI*, 102–108.

Muller-Karger, F., et al. (2001), Annual cycle of primary production in the Cariaco Basin: Response to upwelling and implications for vertical export, *J. Geophys. Res.*, *106*, 4527–4542, doi:10.1029/1999JC000291.

Overpeck, J. T., L. C. Peterson, N. Kipp, J. Imbrie, and D. Rind (1989), Climate change in the circum-North Atlantic region during the last deglaciation, *Nature*, *338*, 553–557, doi:10.1038/338553a0.

Peterson, L. C., and G. H. Haug (2006), Variability in the mean latitude of the Atlantic Intertropical Convergence Zone as recorded by riverine input of sediments to the Cariaco Basin (Venezuela), *Palaeogeogr. Palaeoclimatol. Palaeoecol.*, *234*, 97–113, doi:10.1016/j.palaeo.2005.10.021.

Peterson, L. C., J. T. Overpeck, N. G. Kipp, and J. Imbrie (1991), A high-resolution late Quaternary upwelling record from the anoxic Cariaco Basin, Venezuela, *Paleoceanography*, *6*, 99–119, doi:10.1029/90PA02497.

Peterson, L. C., G. H. Haug, K. A. Hughen, and U. Rohl (2000), Rapid changes in the hydrologic cycle of the tropical Atlantic during the last glacial, *Science*, *290*, 1947–1951, doi:10.1126/science.290.5498.1947.

Rasmussen, S. O., et al. (2006), A new Greenland ice core chronology for the last glacial termination, *J. Geophys. Res.*, *111*, D06102, doi:10.1029/2005JD006079.

Reynolds, L., and R. C. Thunell (1985), Seasonal succession of planktonic-foraminifera in the subpolar North Pacific, *J. Foraminiferal Res.*, *15*, 282–301, doi:10.2113/gsjfr.15.4.282.

Richards, F. A. (1975), The Cariaco Basin (trench), *Oceanogr. Mar. Biol. Annu. Rev.*, *13*, 11–67.

Rohling, E. J., K. Grant, C. Hemleben, M. Kucera, A. P. Roberts, I. Schmeltzer, H. Schulz, M. Siccha, M. Siddall, and G. Trommer (2008), New constraints on the timing of sea level fluctuations during early to middle marine isotope stage 3, *Paleoceanography*, *23*, PA3219, doi:10.1029/2008PA001617.

Schmidt, M. W., and H. J. Spero (2011), Meridional shifts in the marine ITCZ and the tropical hydrologic cycle over the last three glacial cycles, *Paleoceanography*, *26*, PA1206, doi:10.1029/2010PA001976.

Schrader, H., et al. (1980), Laminated diatomaceous sediments from the Guaymas Basin slope (Central Gulf of California): 250,000-year climate record, *Science*, *207*, 1207–1209, doi:10.1126/science.207.4436.1207.

Schubert, C. (1982), Origin of Cariaco Basin, Southern Caribbean Sea, *Mar. Geol.*, *47*, 345–360, doi:10.1016/0025-3227(82)90076-7.

Scranton, M. I., M. McIntyre, G. T. Taylor, F. Muller-Karger, K. Fanning, and Y. Astor (2006), Temporal variability in the nutrient chemistry of the Cariaco Basin, in *Past and Present Marine Water Column Anoxia*, edited by L. N. Neretin, *NATO Sci. Ser., IV*, *64*, 139–160, doi:10.1007/1-4020-4297-3_06.

Siddall, M., E. J. Rohling, A. Almogi-Labin, C. Hemleben, D. Meischner, I. Schmelzer, and D. A. Smeed (2003), Sea-level fluctuations during the last glacial cycle, *Nature*, *423*, 853–858, doi:10.1038/nature01690.

Siddall, M., E. J. Rohling, W. G. Thompson, and C. Waelbroeck (2008), Marine Isotope Stage 3 sea level fluctuations: Data synthesis and new outlook, *Rev. Geophys.*, *46*, RG4003, doi:10.1029/2007RG000226.

Slowey, N. C., and W. B. Curry (1995), Glacial-interglacial differences in circulation and carbon cycling within the upper western North Atlantic, *Paleoceanography*, *10*(4), 715–732, doi:10.1029/95PA01166.

Steig, E. J., E. J. Brooks, J. W. C. White, C. M. Sucher, M. L. Bender, S. J. Lehman, D. L. Morse, E. D. Wassington, and G. D. Clow (1998), Synchronous climate changes in Antarctica and the North Atlantic, *Science*, *282*, 92–95, doi:10.1126/science.282.5386.92.

Tedesco, K. A., and R. C. Thunell (2003a), High resolution tropical climate record for the last 6,000 years, *Geophys. Res. Lett.*, *30*(17), 1891, doi:10.1029/2003GL017959.

Tedesco, K. A., and R. C. Thunell (2003b), Seasonal and interannual variations in planktonic foraminiferal flux and assemblage composition in the Cariaco Basin, Venezuela, *J. Foraminiferal Res.*, *33*, 192–210, doi:10.2113/33.3.192.

Thunell, R. C., and L. A. Reynolds (1984), Sedimentation of planktonic-foraminifera - Seasonal- changes in species flux in the Panama Basin, *Micropaleontology*, *30*, 243–262, doi:10.2307/1485688.

Tudhope, A. W., C. P. Chilcott, M. T. McCulloch, E. R. Cook, J. Chappell, R. M. Ellam, D. W. Lea, J. M. Lough, and G. B. Shimmield (2001), Variability in the El Niño-Southern Oscillation through a glacial-interglacial cycle, *Science*, *291*, 1511–1517, doi:10.1126/science.1057969.

Vink, A., C. Rühlemann, K. Zonneveld, S. Mulitza, M. Hüls, and H. Willems (2001), Shifts in the position of the North Equatorial current and rapid productivity changes in the western tropical Atlantic during the last glaical, *Paleoceanography*, *16*, 479–490, doi:10.1029/2000PA000582.

Voelker, A. H. L. (2002), Global distribution of centennial-scale records for Marine Isotope Stage (MIS) 3: A database, *Quat. Sci. Rev.*, *21*, 1185–1212, doi:10.1016/S0277-3791(01)00139-1.

Wang, C. (2002), Atlantic climate variability and its associated atmospheric circulation cells, *J. Clim.*, *15*, 1516–1536, doi:10.1175/1520-0442(2002)015<1516:ACVAIA>2.0.CO;2.

Wang, C. (2005), ENSO, Atlantic climate variability, and the Walker and Hadley circulations, in *The Hadley Circulation: Present, Past and Future*, edited by H. F. Diaz and R. S. Bradley, pp. 173–202, Kluwer Acad., Amsterdam, doi:10.1007/978-1-4020-2944-8_6.